

Deficit of primitive compositions in binary asteroids and pairs^{*}

K. Minker^{1,2} and B. Carry²

¹ Université Côte d'Azur, Observatoire de la Côte d'Azur, CNRS, Laboratoire Lagrange, France
e-mail: kate.minker@oca.eu

² MAUCA — Master track in Astrophysics, Université Côte d'Azur & Observatoire de la Côte d'Azur, Parc Valrose, 06100 Nice, France

Received November xx, 2022; accepted Month day, year

ABSTRACT

Context. Small binary asteroid systems and pairs are thought to form through fission induced by spin up via the Yarkovsky-O'Keefe-Radzievskii-Paddack (YORP) effect. This process is expected to depend on their structural strength, hence composition.

Aims. We aim to determine how taxonomic classes, used as a proxy for composition, distribute amongst binary asteroids and asteroid pairs compared to the general population.

Methods. We compare the distribution of taxonomic classes of binary systems and pairs with that of a reference sample of asteroids. We build this sample by selecting asteroids to reproduce the orbital and size distribution of the binaries and pairs to minimize potential biases between samples.

Results. A strong deficit of primitive compositions (C, B, P, D types) among binary asteroids and asteroid pairs is identified, as well as a strong excess of asteroids with mafic-silicate rich surface compositions (S, Q, V, A types).

Conclusions. Amongst low mass, rapidly rotating asteroids, those with mafic-silicate rich compositions are more likely to form multiple asteroid systems than their primitive counterparts.

Key words. Minor planets, asteroids: general, Methods: statistical

1. Introduction

Binary systems have long been of interest to astronomers, as a closely orbiting companion can reveal an object's mass, and subsequently density. This is true for any variety of celestial objects, including stars (Herchel, 1832; Hadley, 1903), exoplanetary systems (Bracewell & MacPhie, 1979), and even black holes (Gibbons, 1971). Of course, asteroids pose no exception to this rule, and the possible discovery of asteroids with companions has been discussed since the early 20th century (Weidenschilling et al., 1989). Once the existence of these systems was confirmed with the discovery of Dactyl around (243) Ida in 1993 (Chapman et al., 1995), the detection and characterization of binary asteroid systems, also known as asteroids with satellites, has been a significant point of interest for observers.

Several general populations of binary systems are observed. Many of the earliest identified binaries were large ($D_p > 100$ km) Main-Belt asteroids with small satellites (Merline et al., 2002). A similar population is observed within the Kuiper Belt, alongside a population of large binary systems with two similarly sized components (Fraser et al., 2017). The largest population of known binary systems is composed of small asteroids in the inner solar system with small satellites, which are the focus of the present study.

As of January 10th, 2023, at least 402 binary systems have been identified, and an estimated $15 \pm 4\%$ of near-Earth asteroids (NEAs) are expected to be in binary systems (Pravec et al., 2006; Margot et al., 2015), as are a significant fraction of Main-Belt asteroids. A substantial portion of all known binary asteroid systems share highly similar properties, containing rapidly rotating primaries with spin periods close to the stability limit of 2.4 h, an obliquity approaching 0° or 180° , a secondary to primary diameter ratio of $d_s/d_p \approx 0.3$, a primary diameter of less than 15 km, and a 2:1 relationship between the system semi-major axis and the primary diameter, as can be seen in Figure 1 (or Margot et al., 2015, for a review). These objects are found throughout the inner solar system, and do not include Kuiper Belt objects (KBOs), and account for over 80% of known binary asteroid systems.

These systems are expected to be produced by a common formation mechanism, a rotational-fission model for which was proposed by Walsh et al. in 2008, with variations proposed by Jacobson & Scheeres (2011) and Jacobson et al. (2014). Compositional idiosyncrasies of this population of small, rapidly rotating binary systems are not well studied, but early models by Walsh et al. (2008) suggest that dark taxonomic types would be more likely to form binary systems as a result of their higher porosity. An observational study by Pajuelo et al. (2018) found a deficit of C type NEA binaries, but agreement to the general population within a 1σ uncertainty for all other types. More recently, simulations of the structural evolution of asteroids like Ryugu and Bennu, targets of the

^{*} The catalogs of properties are available at the CDS via anonymous ftp to <http://cdsarc.u-strasbg.fr/> or via <http://cdsarc.u-strasbg.fr/viz-bin/qcat?J/A+A/xxx/Axxx>

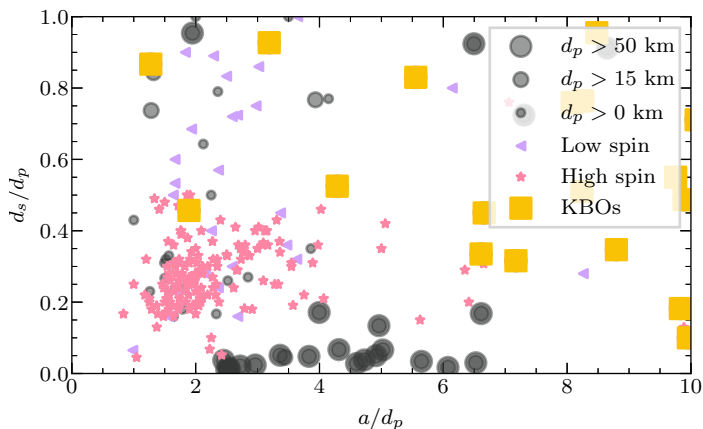


Fig. 1. Known binary systems in the Solar System, including asteroids and Kuiper-belt objects (KBOs). "Low spin" and "High spin" objects, indicated by stars and triangles, are those that have been considered in this study (objects with $D < 15$ km and $a < 2.502$ au). "High spin" objects have a primary rotation period less than 4 h, and "Low spin" objects have primary rotation periods greater than 4 h. The diameter of objects that are not included in the study are indicated by marker size, separated into three sets of $d_p > 50$ km, $50 \text{ km} > d_p > 15$ km, and $d_p < 15$ km. Diameters d_s , d_p , and the system semi-major a are in km.

Hayabusa and OSIRIS-REx missions (Fujiwara et al., 2006; Hamilton et al., 2019), suggest that dark taxonomic types may in fact be less likely to form binary systems at high spin rates, undergoing structural deformation rather than rotational fission under these circumstances (Zhang et al., 2022).

We aim here to establish whether the distribution of taxonomic classes amongst binary systems is similar or different than that of the general asteroid population. In Section 2, we present the data used in this study and the sources from which it was acquired. In Section 3, we discuss how we build a taxonomic reference, by selecting asteroids from the general population. In Section 4, we show the resulting discrepancies in composition between the binary systems and general population. Section 5 provides a discussion of these results.

2. Datasets

In this study, three main populations were considered. First, the 402 known binary asteroids. Second, asteroid pairs, which are expected to have originated as binary systems that are no longer gravitationally bound (Vokrouhlický & Nesvorný, 2008). There are 239 pairs of asteroids suspected to share a common origin, and we mainly consider the primary object of these systems. Finally, the general population, encompassing all known asteroids for which reliable data on their dynamics and composition is available.

In order to construct the largest possible dataset, we included information from a plethora of sources. Using the rocks¹ interface for SsODNet² (Berthier et al., 2022), we gathered values for physical and dynamical parameters of all asteroids considered in this study with full traceability to their original sources, which are outlined in Appendix A.

The list of binary asteroid systems we consider was sourced from Johnston (2019), complemented with updates from the Website³ of the same author, and notices from the Central Bureau for Astronomical Telegrams (CBETs)⁴. The list of pairs was extracted from the recent literature (Vokrouhlický & Nesvorný, 2008; Pravec & Vokrouhlický, 2009; Kyrylenko et al., 2021; Pravec et al., 2019; Vokrouhlický & Nesvorný, 2009; Pravec et al., 2010; Vokrouhlický et al., 2017; Žižka et al., 2016; Rožek et al., 2011; Holt et al., 2020; Moskovitz et al., 2019; Kuznetsov et al., 2020; Vokrouhlický et al., 2022).

From the 402 total binaries and 239 pairs, a subset of 279 binaries and 220 pairs were selected that were likely candidates for formation through the YORP spin mechanism. Two criteria were used for the selection of these objects: first, that the diameter of the systems primary $d_p < 15$ km, and second that the system has a semi-major axis $a < 2.502$ au for binaries or $a < 2.825$ au for pairs, corresponding to objects within the 3:1 and 5:2 mean-motion resonances with Jupiter.

The first excludes larger systems which are unlikely to have formed via the YORP spin mechanism (Polishook et al., 2011). The second limits the set to near-Earth (NEA), Mars-Crossing (MC), Hungaria, Inner Main Belt (IMB) and Middle Main Belt (MMB) populations. These dynamical populations contain the vast majority of small binary systems ($d_p < 15$ km), as a result of efficient targeted surveys (e.g., Warner & Stephens, 2022; Warner, 2015; Warner & Harris, 2012). Additionally, these objects are less likely to be influenced by the incompleteness bias found in the Outer Main Belt (OMB) (Marsset et al., 2022), and are closer to the Sun, therefore in a position to be strongly influenced by the YORP effect (Vokrouhlický et al., 2015). Objects without a known diameter were not rejected from the set, but the diameter of these objects was instead estimated as described in Section 3.

No selection was performed based on the spin period of the primary. While theoretical models (Walsh et al., 2008; Jacobson & Scheeres, 2011) suggest that these systems are formed through rapid rotation, the primary may have reduced spin today due to losing angular momentum in the formation of the secondary, or through decelerating YORP effects (Pravec et al., 2010). Furthermore, easily accessible datasets of spin periods are typically incomplete, and while early reviews of binary systems and binary candidates (Pravec et al., 2006) listed typical spin periods of near-Earth binary systems ranging from 2.2 to 2.8 h, with outliers trailing to 4h, current observations show a much broader range (Warner et al., 2021).

Due to limitations in the size of the binary and pair sets, many taxonomic classes are represented by a low number of systems, such as the Ch, L and E classes. This is compounded when separating the samples by dynamical class. In order to reduce the effects of statistical uncertainties presented by this, in some instances, objects are grouped using a reduced taxonomic classification, where multiple classes are combined (similarly to Mahlke et al., 2021). This is detailed in Table 1. Any objects with a sub-class were classified according to their primary designated; so that an asteroid classified as SI would be considered an S type. This is

¹ <https://rocks.readthedocs.io/>

² <https://ssp.imcce.fr/webservices/ssodnet/>

³ <https://www.johnstonsarchive.net/astro/asteroidmoons.html>

⁴ <http://www.cbat.eps.harvard.edu/cbet/RecentCBETs.html>

Table 1. Taxonomic classes grouped as complexes (Σ), with their average albedo from objects in the spectroscopic set, and the number of binaries (N_b) and pairs (N_p) considered here.

Classes	Σ	p_V	N_b	N_p
S	S	0.24	121	76
Q	Q	0.29	10	3
V	V	0.27	24	13
C, Ch, B, D, P, Z	C	0.05	14	14
E	E	0.52	5	1
K, L, M	M	0.17	12	3

motivated by understandings of known compositional similarities between these classes, such as those highlighted by Vernazza & Beck (2016) or Mahlke et al. (2022).

Although Q type asteroids are similar compositions to S type asteroids (Binzel et al., 2001; Nakamura et al., 2011), they are accounted for separately in the reduced taxonomic classification due to the previously observed overabundance of Q type binary and pair systems (Polishook et al., 2014). While separating objects by dynamical class could reduce some observational biases, doing so is not practical given the current sample size of binary systems. Instead, a reference sample is selected using the methods described in Section 3.

3. Reference population

The selection of an appropriate reference population is essential to understanding the surface composition of binary asteroids. Since a number of observational biases affect the current sample of known binaries, we aim to mimic this population in order to minimize the effects of such biases.

We consider four parameters in the creation of this set; semi-major axis (a), eccentricity (e), inclination (i), and effective diameter (D). These parameters are considered for the following reasons. We include the orbital elements (a, e, i), as it is well known that there is substantial taxonomic variation as a function of these elements (Gradie & Tedesco, 1982; Carvano et al., 2010). The taxonomic distribution of asteroids also shows a substantial dependence on diameter, even when dynamically similar (DeMeo & Carry, 2014). Selection across these parameters minimizes potential biases caused by the over representation of low mass binaries in the population, as well as observational biases from the ease in observing brighter taxonomic types (Stuart & Binzel, 2004; Marsset et al., 2022).

Of the 279 binaries and 220 pairs considered in the present study, 220 binaries and 65 pair primaries have estimates of their effective diameters. We estimate the missing effective diameters (D) from the asteroid absolute magnitude H and the average albedo p_V of their taxonomic class (Table 1) using Equation 1 (Bowell et al., 1989):

$$D = \frac{1329}{\sqrt{p_V}} 10^{-0.2H} \quad (1)$$

We build the reference set as follows, considering as an example the set of known binary asteroids for which taxonomy from spectra are available. We create a four dimensional partition in (a, e, i, D) for the set of binaries. Then, for each object in a box of this partition of space, M objects were randomly selected with replacement for the reference

set from the total population of asteroids within the same variable space. As such, the distribution of selected objects mimic the properties of the binary systems. M is an integer value selected to maximize the size of the reference population while maintaining a reasonable number of instances of object duplication that naturally occurs in boxes with little taxonomic characterisation.

Figure 2 presents a comparison of the properties of the carefully selected reference population with the binary asteroids. The two distributions are extremely similar. This suggests that this method is effective in selecting a reference sample with excellent dynamical similarity to the set of binary systems, therefore reducing the effects of observational biases present in the set of binary asteroids.

Figure 3 compares the carefully selected reference sample using the partitioning method described here with simpler selections. Most notably, there is a substantially higher abundance of C class asteroids in the general population of asteroids with spectra than the carefully selected background. This discrepancy is slightly alleviated when a restriction on the semi-major axis of the background population is imposed, but there is still a strong statistical disagreement. A similar disagreement can be seen in the S class. These discrepancies are due to the non random distribution of asteroid taxonomic classes in the asteroid belt. This has been known for decades (Gradie & Tedesco, 1982), with a higher abundance of primitive types (C/P/D) in the outer belt than in the inner portions of the belt. More recently, it has also been shown that the relative importance of taxonomic classes is not constant with diameter (DeMeo & Carry, 2013, 2014; Bourdelle de Micas et al., 2022). This demonstrates that it is essential to select an appropriate reference population in order to minimize the effects of observational biases affecting both the binary and general populations.

To select an appropriate value of M , it is important to understand the possibility of duplication in the reference sample. Certain areas of the 4D (a, e, i, D) space are significantly emptier than others. Notably, this includes most of the areas in which NEAs are found, which means that these zones are at high risk of excessive duplication when randomly selecting objects in these zones. This could potentially cause significant biases in the reference set, not only increasing the likelihood of over-including binaries in the reference, but could also to extreme over-representation of unusual taxonomic classes that may be present in the space. Because of this, the grid used to build the reference sample cannot be arbitrarily small, and M cannot be arbitrarily large. A large reference sample is, however, ideal to minimize statistical uncertainties, so a small value of M is also undesirable. We examined the duplication rates occurring with several values of M and different partitionings, and ultimately determined that a value of $M = 20$ and boxes of 0.28 au, 0.2, 10.0°, and 1.5 km in (a, e, i, D) provided a reasonable balance between duplication and sample size for this set.

The distribution of duplicated objects is not homogeneous within dynamical classes, largely due to the high prevalence of binary systems within the near-Earth space, and the low percentage of asteroids belonging to that population. This inconsistency could cause a bias towards taxonomic types prevalent amongst NEAs, such as S and Q type asteroids. However, the population with duplicates and without duplicates show a similar taxonomic distribution,

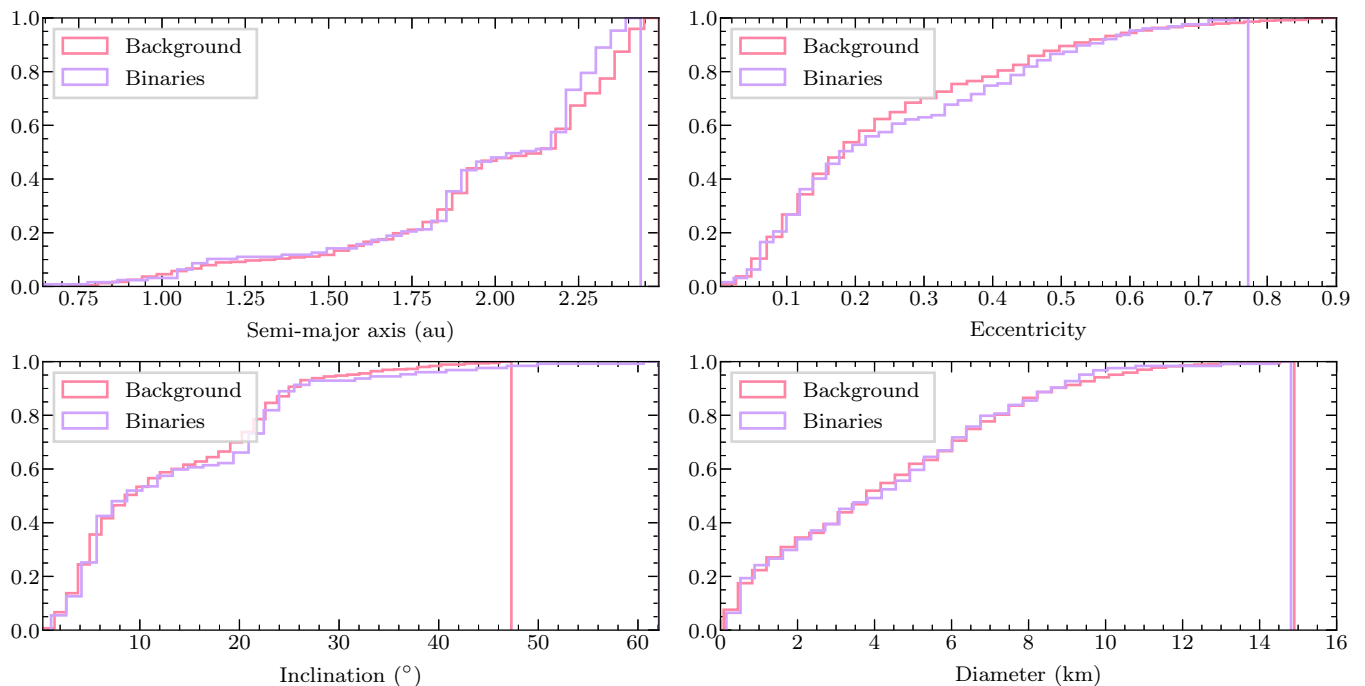


Fig. 2. Cumulative distributions of the semi-major axis, inclination, eccentricity, and diameter of the binary systems (violet) and the selected reference population (red).

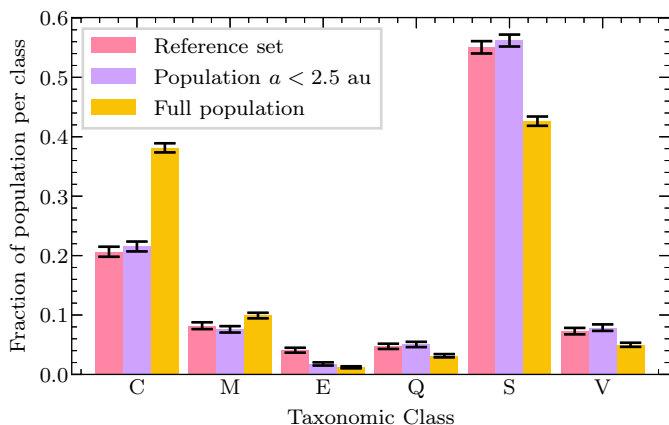


Fig. 3. Illustration of the selection effects on the taxonomic distribution of asteroids. The reference set used hereafter is compared to the entire population of asteroids with taxonomy from spectroscopy, and those which semi-major axis is less than 2.5 au.

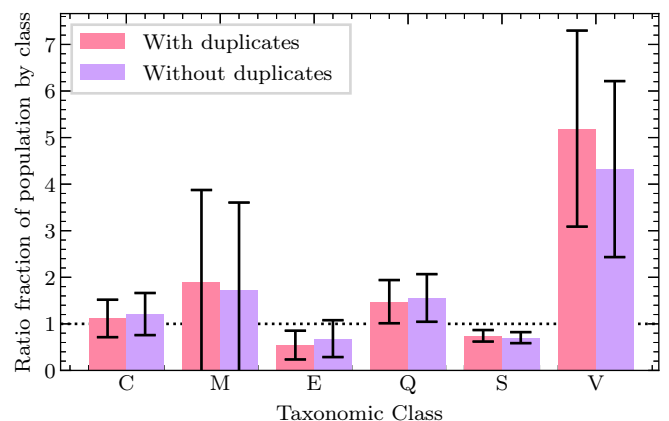


Fig. 4. Ratio of binary systems to the reference sample, amongst NEAs in the spectroscopic set, allowing for duplicates or removing them. The results appear robust against duplication.

as can be seen in Figure 4, suggesting that the bias from the anisotropy of the duplicates is not substantially affecting the distribution of classes. Amongst NEAs where we see the most duplication, the largest discrepancies between the set with duplicates included and the set with duplicates excluded occur in the C and V complexes. Nevertheless, all taxonomic classes show agreement between the sets much below the 1σ level.

To minimize the effects of the inconsistency between different taxonomic schemes, the set of binaries was divided into subsets, those with spectroscopic classifications and those with photometric classifications. Subset membership is mutually exclusive. A separate background population was selected for each of these subsets using the process described above. A similar division was made for the set of

Table 2. M values for the selection of the four reference populations.

Population	Technique	M
Binaries	Spectroscopy	20
Binaries	Photometry	30
Pairs	Spectroscopy	15
Pairs	Photometry	100

asteroid pairs, considering the taxonomy of the primary of the pair, for a total of four subsets and four corresponding reference populations (Table 2). Set membership of asteroids is indicated in Appendix A.

4. Results

4.1. Spectroscopic set

For objects considered in the spectroscopic set, only those with a taxonomy available derived from the method of [Mahlke et al. \(2022\)](#) were considered. The methodology used in this classification is more technically nuanced than previous studies, and accounts for both visible and near-infrared spectra. This classification also accounts for albedo when available, providing another dimension of information, unlike most recent spectroscopic taxonomies ([Bus & Binzel, 2002](#); [DeMeo et al., 2009](#)). Most objects with known spectra are included in this classification. However, only a few thousand objects currently have known spectra⁵, severely limiting the available reference population of this set. Since known binary systems are particularly well represented in the spectroscopic set due to targeted studies by [Pajuelo et al. \(2018\)](#), this set is comparatively more complete, with 127 out of 279 binary systems represented. Pairs are poorly included, with only 36 out of 220 pairs represented ([Polishook et al., 2014](#); [Duddy et al., 2013](#)). We compute the relative incidence of binaries and pairs in the general population by taking the ratio of their taxonomic distribution to that of the reference sample.

We estimate the uncertainties from the statistical error in set membership, as follows:

$$\sigma = \sqrt{\frac{p(1-p)}{n}} \quad (2)$$

where σ is the statistical uncertainty, p is the percentage of the set that a given population occupies, and n is the total number of objects in the set. Standard error propagation techniques then provide the uncertainty in the ratios:

$$\sigma_r = \left| \frac{x}{y} \right| \sqrt{\left(\frac{\sigma_x}{x} \right)^2 + \left(\frac{\sigma_y}{y} \right)^2} \quad (3)$$

where σ_r is the statistical uncertainty in the ratio, x represents the percentages associated with the population of either binaries or pairs, and y represents the percentages associated with the corresponding background population.

The results of this analysis can be seen in [Figure 5](#). There is a significant over-representation of Q and V complex asteroids amongst binary systems, and a significant under-representation of C and M complex asteroids. Amongst pairs, we find a significant under-representation of C and M complex asteroids as well, and a marginal over-representation of S types.

An additional notable finding within this set is the extremely high prevalence of binary systems amongst V type NEAs, with $25 \pm 8\%$ of known V types with associated spectra being known binary systems (7 out of a total of 28). While in agreement with the expected total fraction of binary systems amongst NEAs ($15 \pm 4\%$, [Pravec et al. \(2006\)](#)), this number is unexpectedly high considering the fact that there have been no obvious campaigns to search for binary systems amongst this population and that there

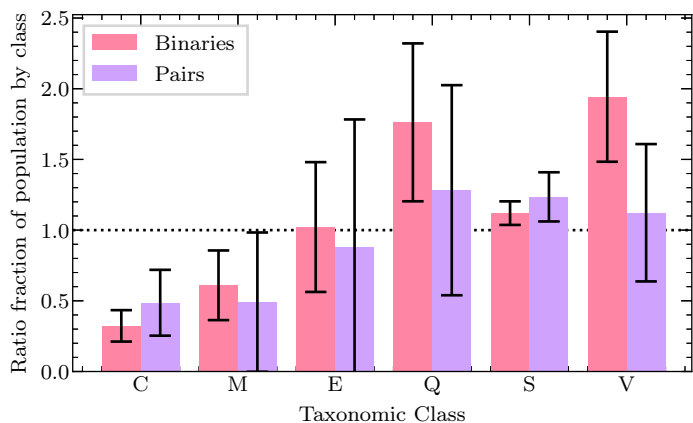


Fig. 5. Taxonomic distribution of binary asteroids relative to the general population, as measured from spectroscopy. A ratio below one indicates an under representation of the class among binaries, while a ratio above one implies that the class is more represented among binaries.

is no reason to assume completeness of the true set of binary systems amongst the currently known population, especially considering the recent discovery of a satellite orbiting V type (7889) 1994 LX in September 2022.

As visible in [Table 3](#), these binaries were discovered by different researchers, both from radar and lightcurve measurements. Since little to no information is available on objects that have been similarly investigated, it is difficult to conclude how many V type NEAs have been searched for satellites without detection. Some of these objects were specifically targeted for spectroscopic studies due to their status as binary systems (such as (348400) 2005 JF21, targeted by [Pajuelo et al., 2018](#)). Still, the high fraction of binary systems that are V types, combined with the high fraction of V type NEAs that are known binaries suggests that there is a striking correlation between the two.

Table 3. Discovery information for V type binary NEAs. Asteroid name and number (Asteroid), year of announcement (Year), discovery technique (Technique), either lightcurve (LC) or radar (Radar), and primary investigator of the discovery (PI).

Asteroid	Year	Technique	PI
(7889) 1994 LX	2022	LC	Warner
(68063) 2000 YJ66	2014	LC	Warner
(164121) 2003 YT1	2004	Radar	Nolan
(348400) 2005 JF21	2015	Radar	Stephens
(357439) 2004 BL86	2015	LC	Pollock
(450894) 2008 BT18	2008	Radar	Benner
(523775) 2014 YB35	2015	Radar	Naidu

4.2. Photometric set

While spectroscopic classification is highly consistent and more nuanced than other methods of taxonomy, the availability of asteroid spectra severely limits its reach.

Although photometric classification schemes can be inconsistent, the number of objects with a photometric classification is significantly larger than that of those with a spectroscopic classification, with recent photometric studies such as [Popescu et al. \(2018\)](#), [Sergeyev & Carry \(2021\)](#),

⁵ Excluding the recent publication of Gaia DR3 visible spectra of 60,000 asteroids ([Gaia Collaboration et al., 2022](#))

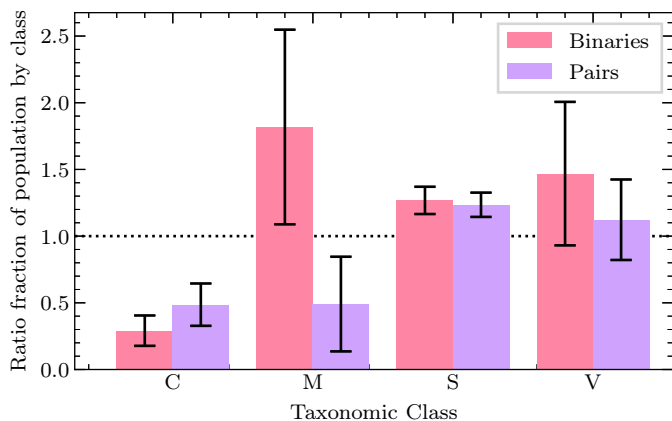


Fig. 6. Taxonomic distribution of binary asteroids relative to the general population, as measured from photometry. Q types are merged with S types in most photometric studies, and thus not separately available.

and [Sergeyev et al. \(2022\)](#) containing over 200,000 objects, while the spectroscopic set of [Mahlke et al. \(2022\)](#) contains only around 4000 asteroids. As such, a much larger number of binary and pair systems have been classified in this manner. Because of this, we study these objects using the technique described for the spectroscopic set, see [Figure 6](#).

We find a significant under-representation of C complex asteroids amongst binary systems, a significant over-representation of S types, and a slight over-representation of M complex asteroids, which are dominated by L type asteroids⁶. We find similar results amongst the pairs, with an additional under-representation of M complex asteroids.

5. Discussion

The results presented in [Figure 5](#) and [Figure 6](#) point to strong differences in the abundance of taxonomic types amongst binary systems compared to the reference population.

We considered the C complex (encompassing C, B, P, and D classes) asteroids to be primitive, due to a shared link between their opaque-rich surface compositions with that of inter-planetary dust particles (IDPs) ([Vernazza et al., 2015](#)). Although P types share spectral similarities to E, M and X type asteroids, and as such are often associated together as an X complex ([Bus & Binzel, 2002; DeMeo et al., 2009](#)), this does not represent a true similarity in composition, and is therefore irrelevant for the purposes of this study. These objects also share characteristics with other remnants of the early Solar System, such as comets ([Elkins-Tanton & Weiss, 2017](#)). We consider an additional super-complex of mafic-silicate rich asteroids, belonging to S, Q, V, and A, as there is evidence for substantial heating in their formation history, sourced from the geologic history of meteorite analogues ([McCord et al., 1970; Vernazza et al., 2014](#)). K, L, M and X classes were not included in either category as these objects are of ambiguous origin (CO/CV and iron meteorites have been proposed as analogs, e.g., [Sunshine et al., 2008; Ockert-Bell et al., 2010; Eschrig et al., 2021](#)), and are not substantially opaque or mafic-silicate rich. X type asteroids encompass objects

⁶ In this case, the M complex contains no M type asteroids.

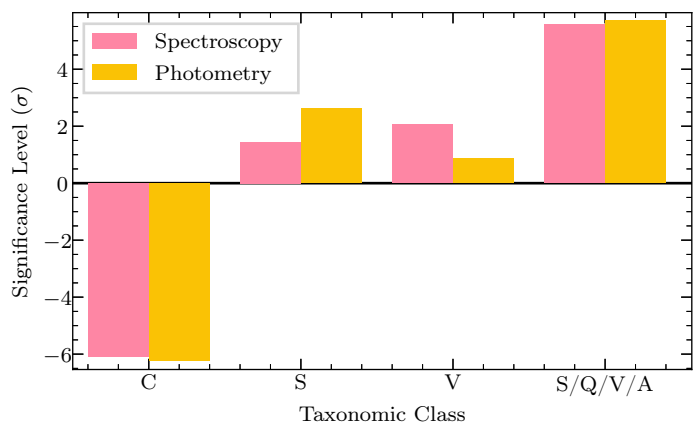


Fig. 7. Number of standard deviation away from the background for selected reduced taxonomic classes, with a negative value representing classes with lower representation in the specified population than the background, and a positive value representing a higher representation in the specified population than the background. Classes are order from least to most thermally evolved moving from left to right, with the most substantial under-representation in the C complex, and the most substantial over-representation in the V class and S/Q/V/A complex.

with no known albedo that could belong to the E, M or P classes, all of which have similar spectral properties but very different compositions ([Bus & Binzel, 2002; DeMeo et al., 2009; Vernazza et al., 2015; Mahlke et al., 2022](#)). M type asteroids have been found to be metal rich, implying that they are from thermally differentiated parent bodies, however, some members of this class have been found to have signatures of silicates or hydration, making the origin of these asteroids ambiguous ([Rivkin et al., 2000; Mahlke et al., 2022](#)).

We compared the relative abundance of asteroids in these categories for the binaries and pairs with respect to their corresponding background populations.

For the spectroscopic set, there was an under abundance of 6.1σ for primitive type asteroids, and an over abundance of 5.6σ for S/Q/V/A type asteroids, suggesting that there is a strong preference for binary formation amongst S, Q, V and A type asteroids, with respect to primitive type asteroids.

Furthermore, in analysis of the reduced taxonomic classes ([Figure 5](#)), it seems that the more thermally evolved the parent body of an asteroid, the more likely it is to form a binary system. This trend can be seen in [Figure 7](#), where the clear increase in standard deviations away from agreement with the background can be seen as the taxonomic groups become increasingly thermally evolved. There is a strong under abundance in the C complex, containing primitive IDPs, and a strong over abundance of V type binary systems, which are associated with the fully differentiated parent body (4) Vesta. This increase is seen across both the photometric and spectroscopic sets.

These findings are in alignment with recent theoretical models based on Hayabusa2 and OSIRIS-REx data by [Zhang et al. \(2022\)](#), which suggest that rapidly rotating asteroids with primitive compositions are more likely to undergo internal deformation than to form binary systems. Our compilation of taxonomic classes for binary systems

and creation of a reference population supports these theoretical predictions.

6. Conclusions

By collecting the taxonomic class for 279 binary asteroids with SsODNet (Berthier et al., 2022), we find significant observational evidence for a non-random distribution of binary systems amongst taxonomic classes. There is an over-representation of multiple asteroids amongst mafic-silicate rich types (Q, V, A, E) and under representation amongst primitive opaque-rich types (C, B, P, D). The high representation of binary systems amongst V type NEAs also suggests that objects forming from further differentiated parent bodies may be more likely to form binaries, but limited sample size leaves this inconclusive. While taxonomies from spectra are valued more highly in this study due to the availability of a low error, highly consistent data set from Mahlke et al. (2022), taxonomies from photometric measurements provide similar results. The taxonomies of 220 asteroid pairs were also considered, based on the primary body of the pairs, and we found that this taxonomic distribution is consistent with that found in the set of binary systems. This is in alignment with recent predictions by Zhang et al. (2022). The consistency between the distributions of binaries and pairs implies that low-albedo taxonomic types have difficulty forming binary systems, rather than difficulty maintaining them.

Acknowledgements. We thank CNES for supporting K. Minker in her internship during her Masters of astrophysics (MAUCA: <http://mauca.oca.eu>). This research used the VO TOPCAT software (Taylor, 2005). The properties of Solar System Object are from the service SsODNet.ssoCard of the Service des éphémérides de l'IMCCE through its Solar System Portal (<https://ssp.imcce.fr>). We thank all the developers and maintainers of resources for the community.

References

- Alf-Lagoa, V. & Delbo', M. 2017, *A&A*, 603, A55
 Berthier, J., Carry, B., Mahlke, M., & Normand, J. 2022, arXiv e-prints, arXiv:2209.10697
 Binzel, R. P., Rivkin, A. S., Bus, S. J., Sunshine, J. M., & Burbine, T. H. 2001, *Meteoritics and Planetary Science*, 36, 1167
 Bourdelle de Micás, J., Fornasier, S., Avdellidou, C., et al. 2022, *A&A*, 665, A83
 Bowell, E., Hapke, B., Domingue, D., et al. 1989, *Asteroids II*, 524
 Bracewell, R. N. & MacPhie, R. H. 1979, *Icarus*, 38, 136
 Bus, S. J. & Binzel, R. P. 2002, *Icarus*, 158, 146
 Carry, B., Solano, E., Eggl, S., & DeMeo, F. E. 2016, *Icarus*, 268, 340
 Carvano, J. M., Hasselmann, P. H., Lazzaro, D., & Mothé-Diniz, T. 2010, *A&A*, 510, A43
 Chapman, C. R., Veveřka, J., Thomas, P. C., et al. 1995, *Nature*, 374, 783
 Delbo, M. 2004, PhD thesis, Free University of Berlin, Germany
 DeMeo, F. E., Binzel, R. P., Slivan, S. M., & Bus, S. J. 2009, *Icarus*, 202, 160
 DeMeo, F. E. & Carry, B. 2013, *Icarus*, 226, 723
 DeMeo, F. E. & Carry, B. 2014, *Nature*, 505, 629
 Duddy, S. R., Lowry, S. C., Christou, A., et al. 2013, *MNRAS*, 429, 63
 Elkins-Tanton, L. T. & Weiss, B. P. 2017, *Planetesimals: Early Differentiation and Consequences for Planets*
 Eschrig, J., Bonal, L., Beck, P., & Prestgard, T. J. 2021, *Icarus*, 354, 114034
 Fraser, W. C., Bannister, M. T., Pike, R. E., et al. 2017, *Nature Astronomy*, 1, 0088
 Fujiwara, A., Kawaguchi, J., Yeomans, D. K., et al. 2006, *Science*, 312, 1330
 Gaia Collaboration, Galluccio, L., Delbo, M., et al. 2022, arXiv e-prints, arXiv:2206.12174
 Gibbons, G. W. 1971, *Nature*, 232, 465
 Gradie, J. & Tedesco, E. 1982, *Science*, 216, 1405
 Hadley, S. M. 1903, *Popular Astronomy*, 11, 240
 Hamilton, V. E., Simon, A. A., Christensen, P. R., et al. 2019, *Nature Astronomy*, 3, 332
 Herchel, John, S. 1832, *MNRAS*, 2, 51
 Holt, T. R., Vokrouhlický, D., Nesvorný, D., Brož, M., & Horner, J. 2020, *MNRAS*, 499, 3630
 Hung, D., Hamuš, J., Masiero, J. R., & Tholen, D. J. 2022, *PSJ*, 3, 56
 Jacobson, S. A. & Scheeres, D. J. 2011, *Icarus*, 214, 161
 Mahlke, M., Carry, B., & Mattei, P. A. 2022, *A&A*, 665, A26
 Johnston, W. R. 2019, *NASA Planetary Data System*, 4
 Kuznetsov, E. D., Rosaev, A. E., Plavalova, E., & Safronova, V. S. 2020, *INASAN Science Reports*, 5, 52
 Kyrlyenko, I., Krugly, Y. N., & Golubov, O. 2021, *A&A*, 655, A14
 Mahlke, M., Carry, B., & Denneau, L. 2021, *Icarus*, 354, 114094
 Mahlke, M., Carry, B., & Mattei, P. A. 2022, *A&A*, 665, A26
 Mainzer, A., Bauer, J., Grav, T., et al. 2014, *ApJ*, 784, 110
 Mainzer, A., Grav, T., Masiero, J., et al. 2012, *ApJ*, 760, L12
 Margot, J. L., Pravec, P., Taylor, P., Carry, B., & Jacobson, S. 2015, in *Asteroids IV*, 355–374
 Marsset, M., DeMeo, F. E., Burt, B., et al. 2022, *AJ*, 163, 165
 Masiero, J. R., Grav, T., Mainzer, A. K., et al. 2014, *ApJ*, 791, 121
 Masiero, J. R., Mainzer, A. K., Bauer, J. M., et al. 2020, *PSJ*, 1, 5
 Masiero, J. R., Mainzer, A. K., Grav, T., et al. 2011, *ApJ*, 741, 68
 Masiero, J. R., Mainzer, A. K., Grav, T., et al. 2012, *ApJ*, 759, L8
 McCord, T. B., Adams, J. B., & Johnson, T. V. 1970, *Science*, 168, 1445
 Merline, W. J., Weidenschilling, S. J., Durda, D. D., et al. 2002, in *Asteroids III*, 289–312
 Moskovitz, N. A., Fatka, P., Farnocchia, D., et al. 2019, *Icarus*, 333, 165
 Mueller, M., Delbo', M., Hora, J. L., et al. 2011, *AJ*, 141, 109
 Myhrvold, N., Pinchuk, P., & Margot, J.-L. 2022, *PSJ*, 3, 30
 Nakamura, T., Noguchi, T., Tanaka, M., et al. 2011, *Science*, 333, 1113
 Nugent, C. R., Mainzer, A., Bauer, J., et al. 2016, *AJ*, 152, 63
 Nugent, C. R., Mainzer, A., Masiero, J., et al. 2015, *ApJ*, 814, 117
 Ockert-Bell, M. E., Clark, B. E., Shepard, M. K., et al. 2010, *Icarus*, 210, 674
 Pajuelo, M., Birlan, M., Carry, B., et al. 2018, *MNRAS*, 477, 5590
 Polishook, D., Brosch, N., & Prialnik, D. 2011, *Icarus*, 212, 167
 Polishook, D., Moskovitz, N., Binzel, R. P., et al. 2014, *Icarus*, 233, 9
 Popescu, M., Licandro, J., Carvano, J. M., et al. 2018, *A&A*, 617, A12
 Pravec, P., Fatka, P., Vokrouhlický, D., et al. 2019, *Icarus*, 333, 429
 Pravec, P., Scheirich, P., Kušnirák, P., et al. 2006, *Icarus*, 181, 63
 Pravec, P. & Vokrouhlický, D. 2009, *Icarus*, 204, 580
 Pravec, P., Vokrouhlický, D., Polishook, D., et al. 2010, *Nature*, 466, 1085
 Rivkin, A. S., Howell, E. S., Lebofsky, L. A., Clark, B. E., & Britt, D. T. 2000, *Icarus*, 145, 351
 Rožek, A., Breiter, S., & Jopek, T. J. 2011, *MNRAS*, 412, 987
 Sergeev, A. V. & Carry, B. 2021, *A&A*, 652, A59
 Sergeev, A. V., Carry, B., Onken, C. A., et al. 2022, *A&A*, 658, A109
 Stuart, J. S. & Binzel, R. P. 2004, *Icarus*, 170, 295
 Sunshine, J. M., Connolly, H. C., McCoy, T. J., Bus, S. J., & La Croix, L. M. 2008, *Science*, 320, 514
 Taylor, M. B. 2005, in *Astronomical Society of the Pacific Conference Series*, Vol. 347, *Astronomical Data Analysis Software and Systems XIV*, ed. P. Shopbell, M. Britton, & R. Ebert, 29
 Trilling, D. E., Mommert, M., Hora, J., et al. 2016, *AJ*, 152, 172
 Trilling, D. E., Mueller, M., Hora, J. L., et al. 2010, *AJ*, 140, 770
 Usui, F., Kuroda, D., Müller, T. G., et al. 2011, *PASJ*, 63, 1117
 Vernazza, P. & Beck, P. 2016, *Planetesimals: Early Differentiation and Consequences for Planets*, ed. L. T. Elkins-Tanton & B. P. Weiss (Cambridge Univ. Press), arXiv:1611.08731
 Vernazza, P., Marsset, M., Beck, P., et al. 2015, *ApJ*, 806, 204
 Vernazza, P., Zanda, B., Binzel, R. P., et al. 2014, *ApJ*, 791, 120
 Vokrouhlický, D., Bottke, W. F., Chesley, S. R., Scheeres, D. J., & Statler, T. S. 2015, in *Asteroids IV*, 509–531
 Vokrouhlický, D., Fatka, P., Micheli, M., Pravec, P., & Christensen, E. J. 2022, *A&A*, 664, L17
 Vokrouhlický, D. & Nesvorný, D. 2008, *AJ*, 136, 280
 Vokrouhlický, D. & Nesvorný, D. 2009, *AJ*, 137, 111
 Vokrouhlický, D., Pravec, P., Durech, J., et al. 2017, *AJ*, 153, 270
 Zizka, J., Galád, A., Vokrouhlický, D., et al. 2016, *A&A*, 595, A20
 Walsh, K. J., Richardson, D. C., & Michel, P. 2008, *Nature*, 454, 188
 Warner, B. D. 2015, *Minor Planet Bulletin*, 42, 132
 Warner, B. D. & Harris, A. 2012, in *AAS/Division for Planetary Sciences Meeting Abstracts*, Vol. 44, *AAS/Division for Planetary Sciences Meeting Abstracts #44*, 110.15
 Warner, B. D., Harris, A. W., & Pravec, P. 2021, *NASA Planetary Data System*, 10
 Warner, B. D. & Stephens, R. D. 2022, *Minor Planet Bulletin*, 49, 223
 Weidenschilling, S. J., Paolicchi, P., & Zappala, V. 1989, in *Asteroids II*, ed. R. P. Binzel, T. Gehrels, & M. S. Matthews, 643–658
 Zhang, Y., Michel, P., Barnouin, O. S., et al. 2022, *Nature Communications*, 13, 4589

Appendix A: Compiled parameters

The majority of data considered in this study was sourced from `SsODNet` (Berthier et al., 2022), which contains a compilation of many independent studies. The exact parameters and objects considered in this study are available electronically at CDS. The first twelve lines of each set are included in this Appendix A. Column headings are as follows, ‘Number’ (asteroid number), ‘Name’ (asteroid name), ‘D’ (primary diameter, if available), ‘ σ_D ’ (uncertainty in primary diameter, if available), ‘D ref’ (reference corresponding to primary diameter, if available), ‘ p_V ’ (albedo, if available), ‘ σ_{p_V} ’ (uncertainty in albedo, if available), ‘Tax. method’ (method for taxonomy, either spectroscopy (spec) or photometry (phot)), ‘Tax. scheme’ (taxonomic scheme), ‘Class’ (taxonomic class), ‘Waverange’ (waverange over which the taxonomy is determined), ‘Tax. Ref’ (reference for the determination of the objects taxonomy). All albedo values are sourced from Berthier et al. (2022), who computed albedo from most-recent absolute magnitudes and best-estimates of diameter, using Equation 1.

Table A.1. Parameters of included objects in the spectroscopic binaries set, first twelve lines included.

Number	Name	D	σ_D	D Ref.	p_V	σ_{p_V}	Tax. method	Tax. scheme	Class	Waverange	Tax. Ref.
1016	Anitra	9.98	0.07	Masiero et al. (2011)	0.3	0.18	Spec	Mahlke	S	VISNIR	Mahlke et al. (2022)
1798	Watts	6.88	0.09	Masiero et al. (2012)	0.24	0.19	Spec	Mahlke	S	VISNIR	Mahlke et al. (2022)
2491	Tvashtri	3.13	0.09	Myhrvold et al. (2022)	0.7	0.19	Spec	Mahlke	A	VISNIR	Mahlke et al. (2022)
2881	Meiden	5.84	0.07	Masiero et al. (2014)	0.27	0.19	Spec	Mahlke	S	VISNIR	Mahlke et al. (2022)
3122	Florence	4.4	0.03	Myhrvold et al. (2022)	0.26	0.18	Spec	Mahlke	S	VISNIR	Mahlke et al. (2022)
3792	Preston	5.13	0.2	Nugent et al. (2016)	0.29	0.2	Spec	Mahlke	S	VISNIR	Mahlke et al. (2022)
4435	Holt	5.56	0.27	Hung et al. (2022)	0.26	0.21	Spec	Mahlke	S	VISNIR	Mahlke et al. (2022)
4666	Dietz	6.73	0.4	Nugent et al. (2016)	0.25	0.22	Spec	Mahlke	A	VISNIR	Mahlke et al. (2022)
7002	Bronshten	3.12	0.31	Alí-Lagoa & Delbo’ (2017)	0.2	0.27	Spec	Mahlke	S	VISNIR	Mahlke et al. (2022)
15745	Yuliya	0.77	0.15	Trilling et al. (2010)	0.32	0.44	Spec	Mahlke	S	VISNIR	Mahlke et al. (2022)
190166	2005 UP156	1.04	0.02	Nugent et al. (2015)	0.2	0.19	Spec	Mahlke	S	VISNIR	Mahlke et al. (2022)
226514	2003 UX34	-	-	-	-	-	Spec	Mahlke	S	VISNIR	Mahlke et al. (2022)

Table A.2. Parameters of included objects in the photometric binaries set, first twelve lines included.

Number	Name	D	σ_D	D Ref.	p_V	σ_{p_V}	Tax. method	Tax. scheme	Class	Waverange	Tax. Ref.
2602	Moore	-	-	-	-	-	Phot	Bus-DeMeo	S	VIS	DeMeo & Carry (2013)
2883	Barabashov	4.96	0.07	Masiero et al. (2014)	0.32	0.19	Phot	Bus-DeMeo	S	VIS	DeMeo & Carry (2013)
5500	Twilley	4.26	0.11	Myhrvold et al. (2022)	0.3	0.19	Phot	Bus-DeMeo	S	VIS	DeMeo & Carry (2013)
6245	Ikufumi	7.88	0.21	Nugent et al. (2016)	0.13	0.19	Phot	Bus-DeMeo	X	VIS	Sergeyev & Carry (2021)
7393	Luginbuhl	5.43	0.1	Nugent et al. (2015)	0.27	0.19	Phot	Bus-DeMeo	S	NIR	Popescu et al. (2018)
9474	Cassadrury	3.57	0.16	Masiero et al. (2011)	0.24	0.21	Phot	Bus-DeMeo	S	VIS	DeMeo & Carry (2013)
18303	1980 PU	-	-	-	-	-	Phot	Bus-DeMeo	S	VIS	Sergeyev et al. (2022)
20882	Paulsanchez	-	-	-	-	-	Phot	Bus-DeMeo	S	VIS	DeMeo & Carry (2013)
25021	Nischaykumar	2.15	0.52	Masiero et al. (2011)	0.16	0.52	Phot	Bus-DeMeo	L	VIS	Sergeyev et al. (2022)
26420	1999 XL103	-	-	-	-	-	Phot	Bus-DeMeo	V	VIS	Sergeyev & Carry (2021)
72036	2000 XM44	3.1	0.58	Nugent et al. (2016)	0.28	0.42	Phot	Bus-DeMeo	S	VIS	Sergeyev et al. (2022)
250162	2002 TY57	-	-	-	-	-	Phot	Bus-DeMeo	S	VIS	Carry et al. (2016)

Table A.3. Parameters of included objects in the photometric pairs set, first twelve lines included.

Number	Name	D	σ_D	D Ref.	p_V	σ_{p_V}	Tax. method	Tax. scheme	Class	Waverange	Tax. Ref.
34380	Pratikvangel	2.2	0.55	Masiero et al. (2011)	0.26	0.53	Phot	Bus-DeMeo	S	VIS	DeMeo & Carry (2013)
38184	1999 KF	2.0	0.37	Masiero et al. (2011)	0.31	0.41	Phot	Bus-DeMeo	S	VIS	DeMeo & Carry (2013)
43008	1999 UD31	-	-	-	-	-	Phot	Bus-DeMeo	S	VIS	Sergeyev et al. (2022)
44620	1999 RS43	-	-	-	-	-	Phot	Bus-DeMeo	S	VIS	Sergeyev et al. (2022)
48652	1995 VB	2.25	0.23	Masiero et al. (2011)	0.23	0.27	Phot	Bus-DeMeo	S	VIS	DeMeo & Carry (2013)
49791	1999 XF31	-	-	-	-	-	Phot	Bus-DeMeo	S	VIS	Sergeyev et al. (2022)
51609	2001 HZ32	1.97	0.67	Masiero et al. (2011)	0.3	0.71	Phot	Bus-DeMeo	V	VIS	Sergeyev et al. (2022)
51866	2001 PH3	3.86	0.12	Nugent et al. (2015)	0.25	0.19	Phot	Bus-DeMeo	S	VIS	Sergeyev et al. (2022)
52478	1995 TO	-	-	-	-	-	Phot	Bus	S	VIS	Carvano et al. (2010)
55764	1992 DG12	-	-	-	-	-	Phot	Bus-DeMeo	A	VIS	Sergeyev et al. (2022)
55913	1998 FL12	-	-	-	-	-	Phot	Bus-DeMeo	X	VIS	Sergeyev et al. (2022)
56700	2000 LL28	-	-	-	-	-	Phot	Bus-DeMeo	S	VIS	DeMeo & Carry (2013)

Table A.4. Parameters of included objects in the spectroscopic pairs set, first twelve lines included.

Number	Name	D	σ_D	D Ref.	p_V	σ_{p_V}	Tax. method	Tax. scheme	Class	Waverange	Tax. Ref.
42946	1999 TU95	4.75	0.1	Masiero et al. (2011)	0.2	0.19	Spec	Mahlke	S	VISNIR	Mahlke et al. (2022)
52852	1998 RB75	2.53	0.38	Masiero et al. (2011)	0.27	0.35	Spec	Mahlke	V	VISNIR	Mahlke et al. (2022)
53537	Zhangyun	-	-	-	-	-	Spec	Mahlke	S	VISNIR	Mahlke et al. (2022)
54041	2000 GQ113	2.68	0.73	Masiero et al. (2011)	0.28	0.57	Spec	Mahlke	V	VISNIR	Mahlke et al. (2022)
54827	Kurpfalz	2.09	0.54	Masiero et al. (2011)	0.24	0.55	Spec	Mahlke	Q	VISNIR	Mahlke et al. (2022)
63440	Rozek	-	-	-	-	-	Spec	Mahlke	C	VISNIR	Mahlke et al. (2022)
74096	1998 QD15	-	-	-	-	-	Spec	Mahlke	S	VISNIR	Mahlke et al. (2022)
88604	2001 QH293	5.8	0.13	Masiero et al. (2011)	0.2	0.19	Spec	Mahlke	S	VISNIR	Mahlke et al. (2022)
92652	2000 QX36	-	-	-	-	-	Spec	Mahlke	S	VISNIR	Mahlke et al. (2022)
101703	1999 CA150	-	-	-	-	-	Spec	Mahlke	S	VISNIR	Mahlke et al. (2022)

Table A.5. Parameters of included objects in the photometric binaries reference set, first twelve lines included.

Number	Name	D	σ_D	D Ref.	p_V	σ_{p_V}	Tax. method	Tax. scheme	Class	Waverange	Tax. Ref.
26920	1996 TQ12	1.52	0.2	Masiero et al. (2011)	0.42	0.33	Phot	Bus-DeMeo	Q	VIS	Sergeyev & Carry (2021)
30577	2001 OU103	1.7	0.2	Masiero et al. (2011)	0.27	0.29	Phot	Bus-DeMeo	S	VIS	Sergeyev et al. (2022)
30958	1994 TV3	1.93	0.1	Masiero et al. (2011)	0.63	0.21	Phot	Bus-DeMeo	C	VIS	DeMeo & Carry (2013)
53428	1999 TD2	-	-	-	-	-	Phot	Bus-DeMeo	X	VIS	Sergeyev et al. (2022)
53440	1999 XQ33	-	-	-	-	-	Phot	Bus	A	VIS	Carvano et al. (2010)
55913	1998 FL12	-	-	-	-	-	Phot	Bus-DeMeo	X	VIS	Sergeyev et al. (2022)
63260	2001 CN	-	-	-	-	-	Phot	Bus-DeMeo	X	VIS	Sergeyev & Carry (2021)
74590	1999 OG2	-	-	-	-	-	Phot	Bus-DeMeo	S	VIS	Sergeyev et al. (2022)
82074	2000 YE119	2.69	0.19	Masiero et al. (2011)	0.22	0.23	Phot	Bus-DeMeo	S	VIS	DeMeo & Carry (2013)
85563	1998 BF7	-	-	-	-	-	Phot	Bus-DeMeo	X	VIS	DeMeo & Carry (2013)
90216	2003 AS85	-	-	-	-	-	Phot	Bus-DeMeo	L	VIS	Sergeyev et al. (2022)
92036	1999 VZ180	-	-	-	-	-	Phot	Bus-DeMeo	X	VIS	Sergeyev & Carry (2021)

Table A.6. Parameters of included objects in the spectroscopic binaries reference set, first twelve lines included.

Number	Name	D	σ_D	D Ref.	p_V	σ_{p_V}	Tax. method	Tax. scheme	Class	Waverange	Tax. Ref.
4581	Asclepius	-	-	-	-	-	Spec	Mahlke	X	VISNIR	Mahlke et al. (2022)
33342	1998 WT24	0.4	0.06	Delbo (2004)	0.67	0.35	Spec	Mahlke	K	VISNIR	Mahlke et al. (2022)
88254	2001 FM129	0.8	0.01	Mainzer et al. (2014)	0.22	0.19	Spec	Mahlke	Q	VISNIR	Mahlke et al. (2022)
138971	2001 CB21	0.34	0.01	Usui et al. (2011)	0.58	0.2	Spec	Mahlke	S	VISNIR	Mahlke et al. (2022)
152563	1992 BF	0.37	0.1	Mainzer et al. (2012)	0.16	0.56	Spec	Mahlke	K	VISNIR	Mahlke et al. (2022)
164202	2004 EW	0.16	0.03	Mueller et al. (2011)	0.31	0.37	Spec	Mahlke	E	VISNIR	Mahlke et al. (2022)
208023	1999 AQ10	0.15	0.04	Trilling et al. (2016)	0.5	0.56	Spec	Mahlke	S	VISNIR	Mahlke et al. (2022)
281375	2008 JV19	-	-	-	-	-	Spec	Mahlke	X	VISNIR	Mahlke et al. (2022)
310442	2000 CH59	-	-	-	-	-	Spec	Mahlke	Q	VISNIR	Mahlke et al. (2022)
401885	2001 RV17	-	-	-	-	-	Spec	Mahlke	S	VISNIR	Mahlke et al. (2022)
474163	1999 SO5	-	-	-	-	-	Spec	Mahlke	S	VISNIR	Mahlke et al. (2022)
518810	2010 CF19	0.08	0.01	Mainzer et al. (2014)	0.47	0.23	Spec	Mahlke	S	VISNIR	Mahlke et al. (2022)

Table A.7. Parameters of included objects in the photometric pairs reference set, first twelve lines included.

Number	Name	D	σ_D	D Ref.	p_V	σ_{p_V}	Tax. method	Tax. scheme	Class	Waverange	Tax. Ref.
163678	2002 XT65	-	-	-	-	-	Phot	Bus-DeMeo	X	VIS	Sergeyev & Carry (2021)
177647	2004 RF110	-	-	-	-	-	Phot	Bus-DeMeo	S	VIS	Sergeyev et al. (2022)
182310	2001 OO43	-	-	-	-	-	Phot	Bus-DeMeo	X	VIS	Sergeyev & Carry (2021)
191919	2005 QS157	-	-	-	-	-	Phot	Bus-DeMeo	S	VIS	DeMeo & Carry (2013)
194922	2002 AK125	-	-	-	-	-	Phot	Bus-DeMeo	B	VIS	Sergeyev et al. (2022)
218019	2001 YX14	-	-	-	-	-	Phot	Bus-DeMeo	S	VIS	Sergeyev et al. (2022)
258019	2001 FY138	-	-	-	-	-	Phot	Bus-DeMeo	S	VIS	Sergeyev et al. (2022)
471448	2011 UZ145	-	-	-	-	-	Phot	Bus-DeMeo	C	VIS	Sergeyev et al. (2022)
475868	2007 CZ12	-	-	-	-	-	Phot	Bus-DeMeo	X	VIS	Sergeyev et al. (2022)
482128	2010 RY1	-	-	-	-	-	Phot	Bus-DeMeo	V	VIS	Sergeyev et al. (2022)
503415	2016 DC2	-	-	-	-	-	Phot	Bus-DeMeo	X	VIS	Sergeyev & Carry (2021)
514044	2014 MM50	-	-	-	-	-	Phot	Bus-DeMeo	X	VIS	Sergeyev & Carry (2021)

Table A.8. Parameters of included objects in the spectroscopic pairs reference set, first twelve lines included.

Number	Name	D	σ_D	D Ref.	p_V	σ_{p_V}	Tax. method	Tax. scheme	Class	Waverange	Tax. Ref.
1920	Sarmiento	2.85	0.16	Masiero et al. (2011)	0.51	0.22	Spec	Mahlke	E	VISNIR	Mahlke et al. (2022)
4736	Johnwood	2.72	0.07	Myhrvold et al. (2022)	0.78	0.19	Spec	Mahlke	E	VISNIR	Mahlke et al. (2022)
6461	Adam	2.6	0.47	Nugent et al. (2016)	0.43	0.41	Spec	Mahlke	E	VISNIR	Mahlke et al. (2022)
7829	Jaroff	2.73	0.16	Masiero et al. (2011)	0.44	0.22	Spec	Mahlke	E	VISNIR	Mahlke et al. (2022)
15692	1984 RA	1.72	0.32	Masiero et al. (2011)	0.58	0.41	Spec	Mahlke	E	VISNIR	Mahlke et al. (2022)
16585	1992 QR	2.0	0.29	Masiero et al. (2011)	0.57	0.35	Spec	Mahlke	E	VISNIR	Mahlke et al. (2022)
20043	Ellenmacarthur	-	-	-	-	-	Spec	Mahlke	S	VISNIR	Mahlke et al. (2022)
25884	Asai	1.91	0.46	Masiero et al. (2011)	0.6	0.52	Spec	Mahlke	E	VISNIR	Mahlke et al. (2022)
53424	1999 SC3	-	-	-	-	-	Spec	Mahlke	S	VISNIR	Mahlke et al. (2022)
138970	2001 CV19	1.09	0.11	Alf-Lagoa & Delbo' (2017)	0.28	0.27	Spec	Mahlke	S	VISNIR	Mahlke et al. (2022)
230269	2001 XZ6	-	-	-	-	-	Spec	Mahlke	S	VISNIR	Mahlke et al. (2022)
275611	1999 XX262	1.48	0.01	Masiero et al. (2020)	0.04	0.18	Spec	Mahlke	Ch	VISNIR	Mahlke et al. (2022)